ADVANCED FUNCTIONAL MATERIALS
www.afm-journal.de



# A Novel Moisture-Insensitive and Low-Corrosivity Ionic Liquid Electrolyte for Rechargeable Aluminum Batteries

*Chi Li, Jagabandhu Patra, Ju Li, Purna Chandra Rath, Ming-Hsien Lin, and Jeng-Kuei Chang**

**Rechargeable aluminum batteries (RABs) are extensively developed due to their cost-effectiveness, eco-friendliness, and low flammability and the earth abundance of their electrode materials. However, the commonly used RAB ionic liquid (IL) electrolyte is highly moisture-sensitive and corrosive. To address these problems, a 4-ethylpyridine/$AlCl_3$ IL is proposed. The effects of the $AlCl_3$ to 4-ethylpyridine molar ratio on the electrode charge–discharge properties are systematically examined. A maximum graphite capacity of 95 mAh $g^{-1}$ is obtained at 25 mA $g^{-1}$. After 1000 charge–discharge cycles, ≈85% of the initial capacity can be retained. In situ synchrotron X-ray diffraction is employed to examine the electrode reaction mechanism. In addition, low corrosion rates of Al, Cu, Ni, and carbon-fiber paper electrodes are confirmed in the 4-ethylpyridine/$AlCl_3$ IL. When opened to the ambient atmosphere, the measured capacity of the graphite cathode is only slightly lower than that found in a $N_2$-filled glove box; moreover, the capacity retention upon 100 cycles is as high as 75%. The results clearly indicate the great potential of this electrolyte for practical RAB applications.**

## 1. Introduction

To utilize intermittent renewable energy sources, large-scale energy storage is required,[1,2] and secondary batteries with high charge–discharge efficiency, low cost, and good safety are appealing. Li-ion batteries (LIBs), the dominant type of energy storage in consumer electronic devices, may not be a good candidate due to the high cost of Li precursors and their uneven distribution in the earth's crust.[3,4] In addition, there are safety concerns associated with the highly volatile and flammable carbonate electrolyte in LIBs.[5] This safety risk can increase for large systems because numerous cells are densely stacked and thermal runaway can thus spread more easily.[6,7] Therefore, an alternative energy storage device that is safe and inexpensive is desirable.[8]

Rechargeable aluminum batteries (RABs) have recently received research attention owing to their potentially low cost and environmental friendliness, the high abundance of aluminum, and the three-electron transfer mechanism at the anode.[9] Dai and co-workers proposed a RAB based on an Al metal anode, a graphite cathode, and a nonflammable 1-ethyl-3-methylimidazolium chloride (EMICl)–aluminum chloride ($AlCl_3$) ionic liquid (IL) electrolyte.[10] Al metal deposition/stripping at the anode and $AlCl_4^-$ anion intercalation/deintercalation at the cathode occur during charging/discharging. This RAB was able to discharge at a voltage plateau near 2 V with a graphite-based capacity and a Coulombic efficiency (CE) of ≈70 mAh $g^{-1}$ and 98%, respectively. In addition, ultrafast charging (at a current density of ≈4000 mA $g^{-1}$, around one minute) was achieved. These results demonstrated the potential of RABs for practical applications. To improve the performance of RABs, several kinds of cathode, including modified graphites,[10–12] graphene nanosheets,[13–15] carbon-based materials,[16–18] transition metal oxides,[19–21] and metal sulfides,[22–25] have been developed. However, the IL electrolyte has received much less attention.

An electrolyte plays a crucial role in determining the battery charge–discharge behavior, cycling stability, and safety properties.[26,27] For RABs, the commonly used electrolyte is EMICl–$AlCl_3$ IL with an $AlCl_3$ to EMICl molar ratio of greater than 1.[10,28–30] This Lewis acid IL, which consists of $EMI^+$, $AlCl_4^-$

C. Li, Prof. J.-K. Chang
Institute of Materials Science and Engineering
National Central University
300 Jhong-Da Road, Taoyuan 32001, Taiwan
E-mail: jkchang@nctu.edu.tw

Dr. J. Patra, Prof. J.-K. Chang
Hierarchical Green-Energy Materials (Hi-GEM) Research Center
National Cheng Kung University
1 University Road, Tainan 70101, Taiwan

The ORCID identification number(s) for the author(s) of this article can be found under https://doi.org/10.1002/adfm.201909565.

DOI: 10.1002/adfm.201909565

Dr. J. Patra, Dr. P. C. Rath, Prof. J.-K. Chang
Department of Materials Science and Engineering
National Chiao Tung University
1001 University Road, Hsinchu 30010, Taiwan

Prof. J. Li
Department of Nuclear Science and Engineering and Department of Materials Science and Engineering
Massachusetts Institute of Technology
77 Massachusetts Ave, Cambridge, MA 02139, USA

Prof. M.-H. Lin
Department of Chemical and Materials Engineering
Chung Cheng Institute of Technology
National Defense University
1000 Xingfeng Road, Taoyuan 334, Taiwan

 

(for intercalation/deintercalation toward the graphite positive electrode), and $Al_2Cl_7^-$ (for deposition/stripping of Al at the negative electrode), enables charge–discharge redox reactions of the Al//graphite RAB.[31,32] Some studies have shown that urea–$AlCl_3$ IL, which is less expensive than EMICl–$AlCl_3$, can also work for Al//graphite RABs.[33–35] At room temperature, a specific cathode capacity of ≈73 mAh $g^{-1}$ was obtained. A high CE over a range of charge–discharge rates (50–200 mA $g^{-1}$) and high stability over 200 cycles were also demonstrated.[33] At ≈120 °C, the graphite capacity can be improved to ≈94 mAh $g^{-1}$.[34,35] Li et al. found that introducing EMICl into urea–$AlCl_3$ IL (to make a ternary mixture) can increase the electrolyte conductivity and thus the charge–discharge properties of the graphite cathode.[36] Chloroaluminate IL electrolytes with inorganic cations have also been developed for RABs. For instance, NaCl–$AlCl_3$ and NaCl–KCl–$AlCl_3$ have been proposed.[37,38] These inorganic ILs (or molten salts) have relatively high melting points (the eutectic points are above 100 °C), and thus the RAB operation temperature is usually limited to ≈120 °C. It should be emphasized that all the above electrolytes are moisture-sensitive (react with $H_2O$ to produce chlorooxoaluminate (III) species and HCl gas).[39] This not only complicates electrolyte handling and cell assembly but also increases the risk to safety. In this context, an alternative IL electrolyte that can operate at room temperature and is moisture-insensitive is highly desirable.

The strong corrosivity of conventional chloroaluminate ILs[40–42] is a problem for RABs. The $Al_2Cl_7^-$ anions are believed to be mainly responsible for this corrosivity. Moreover, these $Al_2Cl_7^-$ anions travel against the electric field and the IL cations at the negative electrode under a reduction potential for Al electrodeposition (e.g., 4 $Al_2Cl_7^-$ + 3 $e^-$ → Al + 7 $AlCl_4^-$). This induces polarization and reduces the energy efficiency of charging the RABs. Therefore, our goal is to develop an IL electrolyte with aluminum-containing cations as the electroactive species to replace $Al_2Cl_7^-$. In the present work, a neutral ligand, 4-ethylpyridine, is reacted with $AlCl_3$ (with various molar ratios) to form a new IL electrolyte. In addition to the electrodeposition/stripping of Al, the charge–discharge properties of a graphite electrode in this series of IL electrolytes are investigated for the first time. The air stability and corrosion properties of the IL are also examined. In situ synchrotron X-ray diffraction (XRD) analysis is carried out to study the reaction stage of the graphite cathode.

## 2. Results and Discussion

The scanning electron microscopy (SEM) and XRD data of the natural graphite powder are shown in Figure S1 of the Supporting Information. The flake-like graphite was found to have an average lateral size of ≈150 µm. The notable XRD peaks at 26.6° and 54.7° can be ascribed to the graphite (002) and (004) plane diffractions, respectively. The calculated $d_{002}$ interplanar spacing is 0.335 nm, which indicates an ideal graphitic structure.

Various $AlCl_3$ to 4-ethylpyridine molar ratios (from 1.1:1 to 1.4:1) were used to prepare the IL electrolytes. The liquids were optically transparent, dark yellow, and highly fluidic. It was found that when the $AlCl_3$/4-ethylpyridine molar ratio was

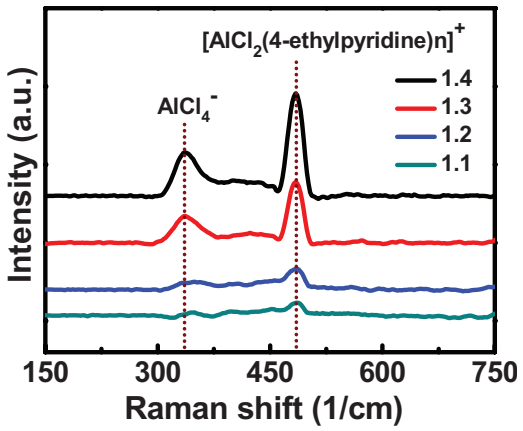


**Figure 1.** Raman spectra of 4-ethylpyridine–$AlCl_3$ IL electrolytes with various $AlCl_3$/4-ethylpyridine molar ratios.

1.4, the $AlCl_3$ powder could not be completely dissolved in the IL due to the solubility limit (see Figure S2, Supporting Information). The Raman data in **Figure 1** show two distinct peaks at 347 and 490 $cm^{-1}$, corresponding to $AlCl_4^-$ and $[AlCl_2(4\text{-ethylpyridine})_n]^+$, respectively.[43,44] According to Equation (1), $AlCl_3$ reacts with 4-ethylpyridine to form $[AlCl_2(4\text{-ethylpyridine})_2]^+$ and $AlCl_4^-$.[45] The further added $AlCl_3$ could asymmetrically dissociate into positive $AlCl_2^+$ and negative $AlCl_4^-$ species, as shown in Equation (2). Equation (3) shows that $AlCl_2^+$ can then react with $[AlCl_2(4\text{-ethylpyridine})_2]^+$ to generate $[AlCl_2(4\text{-ethylpyridine})]^+$.[45] As a result, the intensity of both peaks in the Raman spectra become stronger with increasing $AlCl_3$ concentration

$$2\,AlCl_3 + 2\,4\text{-ethylpyridine} \rightarrow \left[AlCl_2\left(4\text{-ethylpyridine}\right)_2\right]^+ + AlCl_4^- \quad (1)$$

$$2\,AlCl_3 \rightarrow AlCl_2^+ + AlCl_4^- \quad (2)$$

$$AlCl_2^+ + [AlCl_2(4\text{-ethylpyridine})_2]^+ \rightarrow 2\,[AlCl_2(4\text{-ethylpyridine})]^+ \quad (3)$$

It should be emphasized that regardless of the $AlCl_3$ to 4-ethylpyridine ratio, there is no $Al_2Cl_7^-$ anion, which exhibits Raman signals at 309 and 430 $cm^{-1}$,[43,44] in the ILs.

**Table 1** shows the ionic conductivity values of the 4-ethylpyridine–$AlCl_3$ IL electrolytes acquired at 25 °C. The measured conductivity of the IL with an $AlCl_3$/4-ethylpyridine molar ratio of 1.1 was 0.71 mS $cm^{-1}$. With increasing $AlCl_3$ ratio, the

**Table 1.** Ionic conductivity, viscosity, and density values of 4-ethylpyridine–$AlCl_3$ IL electrolytes with various $AlCl_3$ to 4-ethylpyridine molar ratios measured at 25 °C.

| $AlCl_3$/4-ethylpyridine molar ratio | Conductivity [mS $cm^{-1}$] | Viscosity [mPa s] | Density [g $cm^{-3}$] |
|---|---|---|---|
| 1.1 | 0.71 | 17.80 | 1.209 |
| 1.2 | 0.78 | 19.62 | 1.214 |
| 1.3 | 0.89 | 22.36 | 1.216 |
| 1.4 | 0.91 | 23.57 | 1.217 |

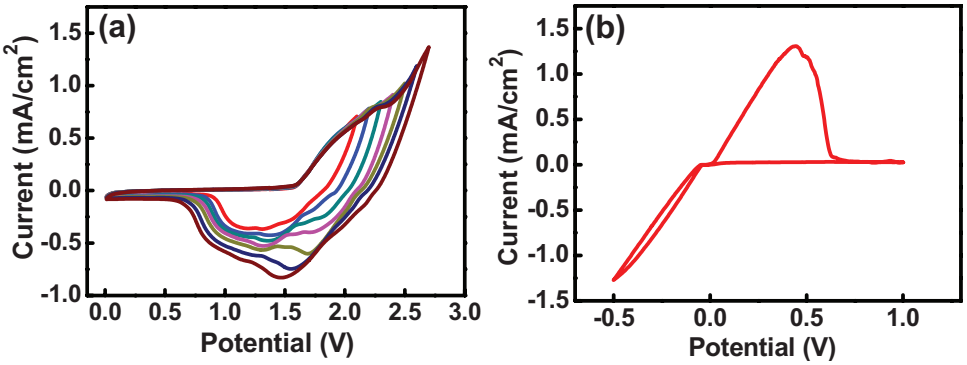


**Figure 2.** CV curves of a) graphite electrode and b) glassy carbon electrode measured at 25 °C in IL electrolyte with $AlCl_3$/4-ethylpyridine molar ratio of 1.3. The potential sweep rate is 1 mV $s^{-1}$.

numbers of cations and anions increased (Equations (1)–(3)), leading to improved ionic conductivity. The conductivity value for the IL with an $AlCl_3$/4-ethylpyridine molar ratio of 1.4 was 0.91 mS $cm^{-1}$. Also shown in Table 1 is that the viscosity of the ILs slightly increases with the $AlCl_3$/4-ethylpyridine ratio (from 17.8 to 23.6 mPa s), probably due to enhanced interactions (or aggregations) between ions when their concentrations are high. It was found that the conductivity and viscosity of the 4-ethylpyridine–$AlCl_3$ IL are more favorable than those of 4-propylpyridine–$AlCl_3$ IL (0.5 mS $cm^{-1}$ and 42.8 mPa s at room temperature for IL with an $AlCl_3$/4-propylpyridine molar ratio of 1.3) reported in the literature.[45] This can be ascribed to the shorter chain length of 4-ethylpyridine compared with that of 4-propylpyridine. It is also found that the density of the IL increases from 1.209 to 1.217 g $cm^{-3}$ when the $AlCl_3$/4-ethylpyridine ratio increases from 1.1 to 1.4 (Table 1).

**Figure 2**a shows the cyclic voltammetry (CV) curves of the natural graphite electrode recorded in the IL electrolyte with an $AlCl_3$/4-ethylpyridine ratio of 1.3 at a potential sweep rate of 1 mV $s^{-1}$. During the positive scans, anodic humps, which are attributed to different stages of $AlCl_4^-$ intercalation into the graphite, were observed. When the potential was scanned backward, reversible deintercalation of the anions took place.[46,47] A high CE (≈99%) was found up to 2.3 V (vs Al), indicating high redox reversibility within this potential range. When the potential was above 2.3 V, another side reaction (probably due to electrolyte breakdown) occurred, leading to a CE reduction (e.g., 87.5% at 2.7 V). This irreversible decomposition should be avoided during RAB operation. Figure S3 of the Supporting Information confirms that the current contributed from the carbon-fiber paper substrate is negligible.

Figure 2b shows the CV curves of a glassy carbon electrode measured in a potential range of −0.5 to 1.0 V in the IL electrolyte with an $AlCl_3$/4-ethylpyridine ratio of 1.3. During the negative scan, electrodeposition of Al started at ≈−0.05 V. A corresponding Al stripping peak emerged at ≈0 V when the potential was scanned toward positive values. The following redox transition is expected, whose reaction mechanism is similar to that of $AlCl_3$–amide IL systems.[48]

$$2\,[AlCl_2(\text{4-ethylpyridine})_n]^+ + 3e^- \leftrightarrow Al + AlCl_4^- + 2n\ \text{4-ethylpyridine} \quad (4)$$

It was confirmed that the electrodeposition/anodic stripping of Al was highly reversible (≈99% CE). These results reveal that the IL based on the complexation of neutral 4-ethylpyridine ligands and $AlCl_3$ is a promising candidate for RAB applications. The CV curves measured with other $AlCl_3$/4-ethylpyridine ratios are shown in Figure S4 of the Supporting Information. When the ratio is lower than 1.1, the reversible Al deposition/stripping becomes unfeasible.

The galvanostatic charge–discharge curves of Al//graphite cells with various 4-ethylpyridine–$AlCl_3$ IL electrolytes are shown in **Figure 3**a–d. The charge cut-off voltage was set at 2.2 V to avoid electrolyte decomposition side reactions. The average operation voltage was ≈1.8–1.9 V with a high charge–discharge CE. At a low current density of 25 mA $g^{-1}$, the measured reversible capacities were 41, 55, 95, and 80 mAh $g^{-1}$, respectively, for the cells with $AlCl_3$/4-ethylpyridine molar ratios of 1.1, 1.2, 1.3, and 1.4. When the charge–discharge rate was increased to 300 mA $g^{-1}$, the capacities decreased to 8, 14, 30, and 21 mAh $g^{-1}$, corresponding to 20%, 25%, 32%, and 26% retention compared with the values measured at 25 mA $g^{-1}$, respectively. With increasing $AlCl_3$ proportion, the concentration of $[AlCl_2(\text{4-ethylpyridine})_n]^+$ cations increased; these cations are electroactive species for Al eletrodepositing/stripping at the anode. Meanwhile, the $AlCl_4^-$ concentration also increased according to Equations (1) and (2). The $AlCl_4^-$ anions are considered the major intercalants for the graphite cathode.[31,37] In addition, as shown in Table 1, the electrolyte conductivity increases with the $AlCl_3$ molar ratio. As a result, the cell charge–discharge performance continuously improved until the $AlCl_3$/4-ethylpyridine ratio increased to 1.3. With this electrolyte, as shown in Figure 3c, the upper voltage plateau (above 2 V) becomes obvious, which indicates that the $AlCl_4^-$ intercalation reaction toward the graphite electrode is promoted, leading to the superior capacities. When the $AlCl_3$ ratio was further increased, the capacity and rate capability of the cell decreased (see Figure 3e). This could be attributed to increased viscosity (see Table 1) and the precipitates in the electrolyte (see Figure S2, Supporting Information); both are unfavorable for battery performance. Of note, this is the first work to develop an $Al_2Cl_7^-$-free, neutral ligand (4-ethylpyridine)–$AlCl_3$ IL electrolyte for RAB applications. The charge–discharge curves of an Al//graphite cell with 4-propylpyridine–$AlCl_3$ IL electrolyte are shown in Figure S5 of the Supporting Information. The

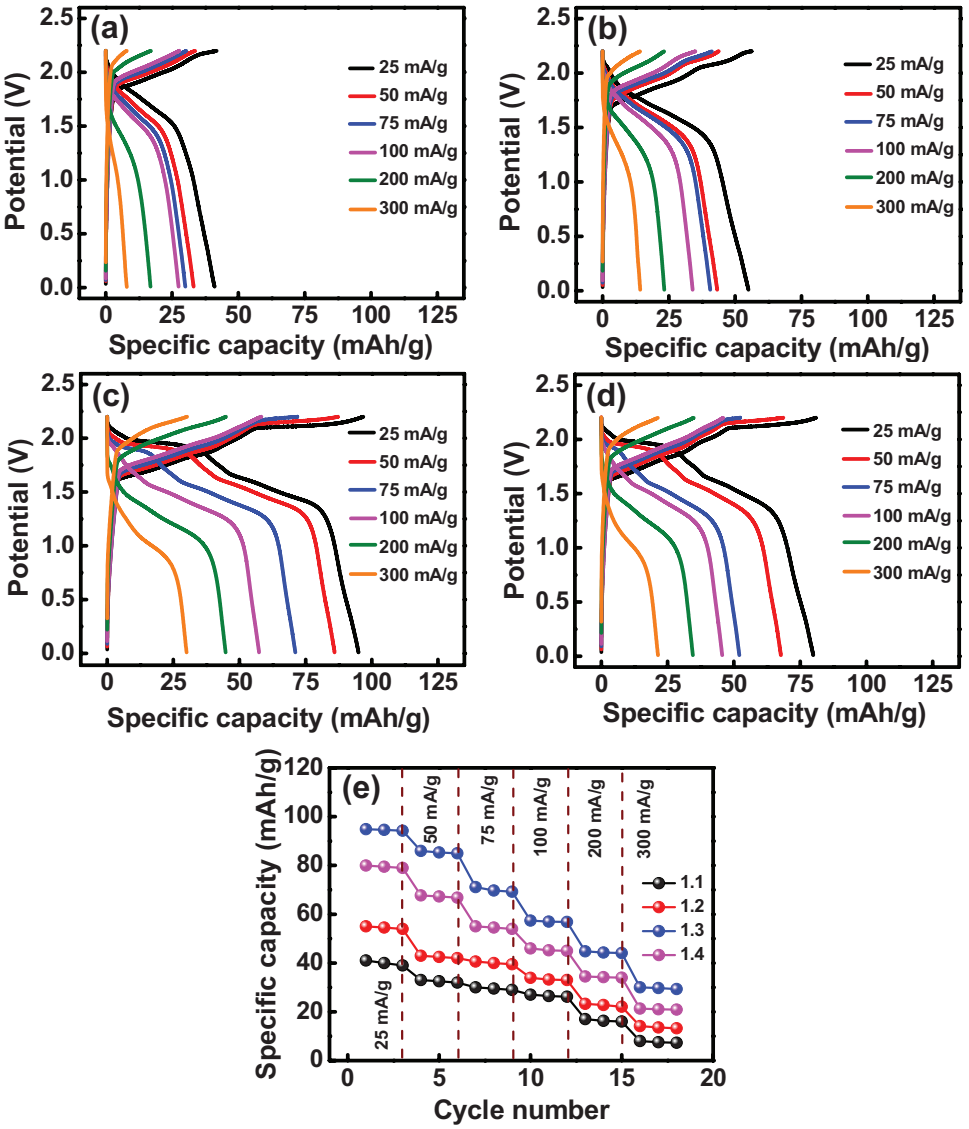


**Figure 3.** Galvanostatic charge–discharge curves of Al//graphite cells containing IL electrolytes with $AlCl_3$/4-ethylpyridine molar ratios of a) 1.1, b) 1.2, c) 1.3, and d) 1.4 measured at 25 °C. e) Comparison of reversible capacities of various cells measured at various rates.

capacities are inferior to those found for the 4-ethylpyridine–$AlCl_3$ cell.

Figure S6 of the Supporting Information shows that the IL with an $AlCl_3$/4-ethylpyridine molar ratio of 1.3 is stable and remains liquid over a wide temperature range. The exact temperature window of this electrolyte needs further study and will be detailed elsewhere.

Electrochemical impedance spectroscopy (EIS) was used to further examine the cell impedance properties. The obtained data (after five conditioning charge–discharge cycles) are shown in **Figure 4**a. The Nyquist spectra are composed of a semicircle at high frequency and a sloping line at low frequency, which can be characterized by the equivalent circuit shown in the figure inset, where $R_e$, $R_{ct}$, *CPE*, and *W* are the electrolyte resistance, interfacial charge transfer resistance, interfacial constant phase element, and Warburg impedance associated with $AlCl_4^-$ transport in the graphite electrode, respectively. It is found that the $R_{ct}$ values, corresponding to the diameters of the EIS semicircles, are 1522, 1050, 545, and 708 Ω, respectively, for the cells with $AlCl_3$/4-ethylpyridine molar ratios of 1.1, 1.2, 1.3, and 1.4. Even though we avoided undissolved particles (see Figure S2, Supporting Information) from the IL with an $AlCl_3$/4-ethylpyridine ratio of 1.4 during cell assembly, some precipitates can form during charge–discharge and thus may occupy the electrode surface, hindering the charge transfer reactions. This probably contributed to the deteriorated cell charge–discharge performance when the $AlCl_3$ molar ratio was excessive.

The cycling stability of Al//graphite cells with various 4-ethylpyridine–$AlCl_3$ IL electrolytes was evaluated using 1000 charge–discharge cycles (at a rate of 100 mA $g^{-1}$). Figure 4b shows the obtained data for the cell containing the IL with an $AlCl_3$/4-ethylpyridine ratio of 1.3. The data for the other cells are shown in Figure S7 of the Supporting Information. All cells show

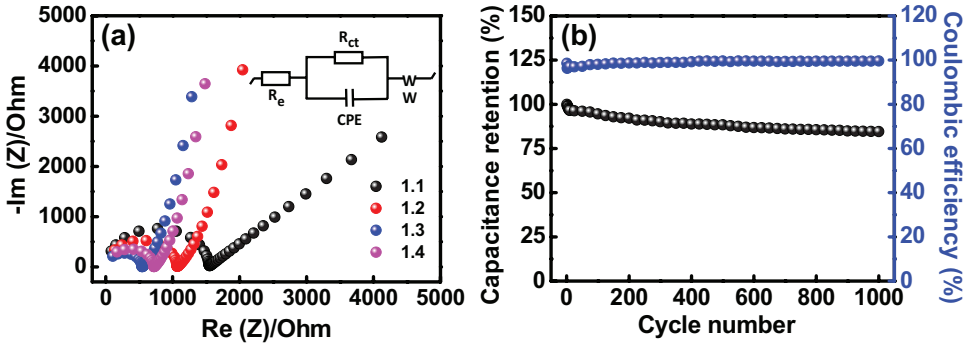


**Figure 4.** a) Nyquist spectra of Al//graphite cells containing IL electrolytes with various $AlCl_3$/4-ethylpyridine molar ratios. b) Cycling stability of Al//graphite cell containing IL electrolyte with $AlCl_3$/4-ethylpyridine molar ratio of 1.3 measured at 25 °C.

very similar stability regardless of the electrolyte composition. Typically, the capacity retention was ≈85% after 1000 charge–discharge cycles with the CE stabilizing at ≈99.5%. Figure S8 of the Supporting Information compares the EIS spectra before and after cycling. The increase of the Warburg impedance (i.e., ion transport resistance) seems to be the main reason for the electrode performance decay.

X-ray photoelectron spectroscopy (XPS) was used to examine the chemical composition of the graphite cathode in charged and discharged states. The obtained spectra are shown in **Figure 5**. The IL electrolyte with an $AlCl_3$/4-ethylpyridine ratio of 1.3 was used. In the charged state, the C 1s peak developed a new shoulder at 285.9 eV (Figure 5a). This confirms the electrochemical oxidation of the graphite via the intercalation of $AlCl_4^-$ anions. The intercalation of the chloroaluminate ions between the graphitic layers was also evidenced by the emergence of Al 2p and Cl 2p peaks upon charging (Figure 5b,c). The Cl 2p peak consists of $2p_{1/2}$ and $2p_{3/2}$ signals, resulting in the asymmetric shape. As shown, the C 1s peak recovers to that of the pristine graphite and the Al 2p and Cl 2p signals significantly diminish upon discharging, indicating deintercalation of $AlCl_4^-$ from the graphite. The charge–discharge redox reaction of the graphite electrode can thus be expressed as shown below

$$C_n + AlCl_4^- \leftrightarrow C_n[AlCl_4] + e^- \quad (5)$$

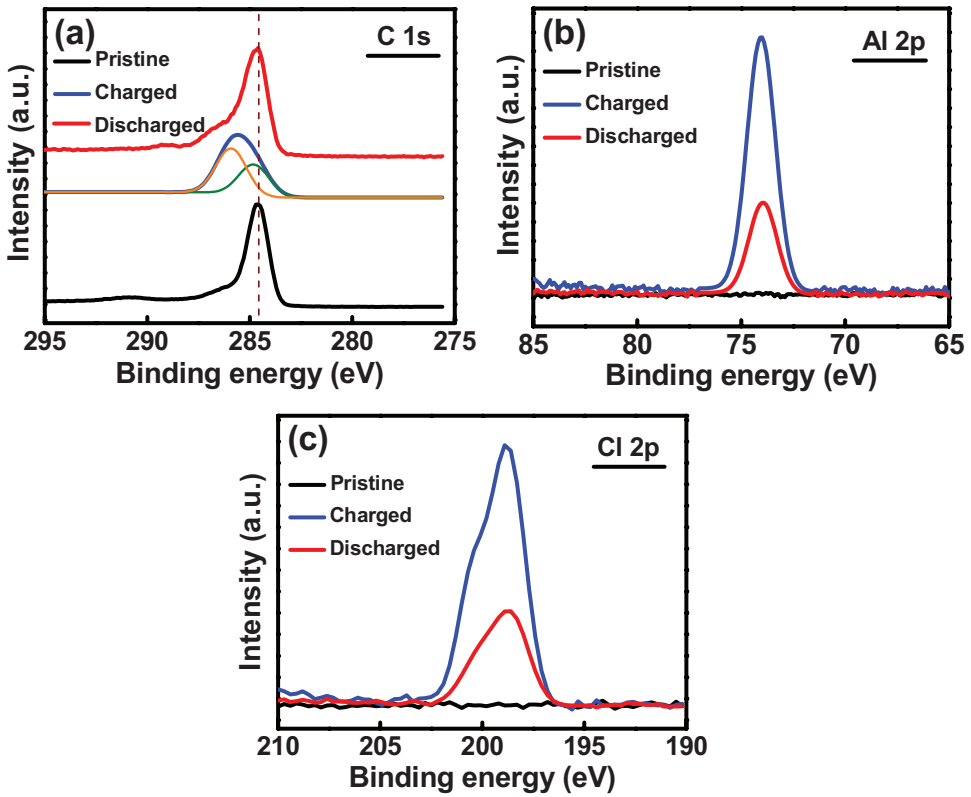


**Figure 5.** XPS a) C 1s, b) Al 2p, and c) Cl 2p spectra of pristine, charged, and discharged graphite electrodes performed in IL electrolyte with $AlCl_3$/4-ethylpyridine molar ratio of 1.3.

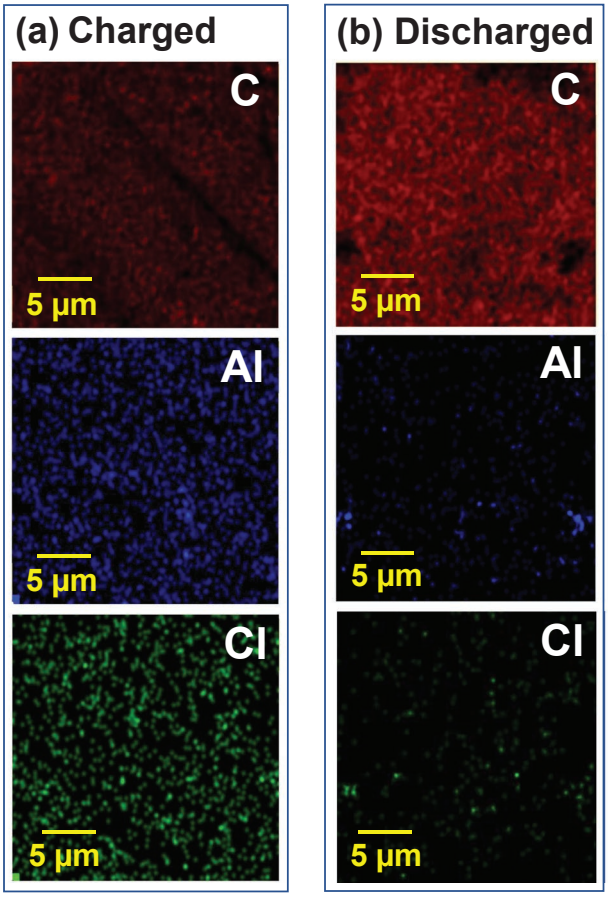


**Figure 6.** EDS mapping of graphite cathodes in a) charged and b) discharged states performed in IL electrolyte with $AlCl_3$/4-ethylpyridine molar ratio of 1.3.

The remaining Al and Cl signals observed in the discharged state were attributed to trapped species in the graphite structure and/or residual electrolyte on the electrode surface. In addition, energy-dispersive X-ray spectroscopy (EDS) mapping was conducted to further examine the graphite reaction mechanism. As shown in **Figure 6**a, Al and Cl elements were uniformly distributed over the electrode in the charged state, confirming $AlCl_4^-$ intercalation. Figure 6b shows that these chloroaluminate ions were extracted after discharging.

In situ synchrotron XRD analysis was performed on the Al// graphite pouch cell. **Figure 7** shows a series of diffraction patterns of the graphite electrode collected in the IL electrolyte with an $AlCl_3$/4-ethylpyridine ratio of 1.3 at various potentials. The pristine sharp (002) peak at 26.6° gradually diminished upon charging, whereas two new peaks, around 22.8° and 27.3°, respectively, emerged at 1.7 V. The two peaks shifted toward lower and higher angles, respectively, and their intensity increased upon charging. The split XRD peaks suggested that highly strained graphene stacks formed due to the anion intercalation. Gao et al.[49] predicted from first-principles calculations that two $AlCl_4^-$ ions intercalated into the graphite together by a standing tetrahedral geometry, which led to interlayer expansion. The two new XRD peaks can be associated with (0 0 $n$+1) and (0 0 $n$+2) reflections, respectively, where $n$

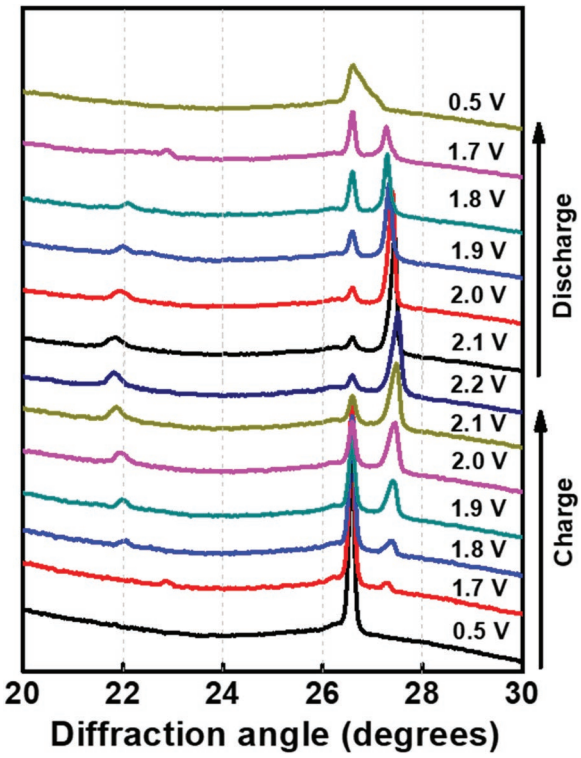


**Figure 7.** In situ synchrotron XRD patterns of graphite cathode taken at various charge–discharge potentials in IL electrolyte with $AlCl_3$/4-ethylpyridine molar ratio of 1.3.

represents the stage number of the graphite intercalation compound (GIC).[50] At 1.7 V, the calculated $d_{(0\ 0\ n+1)}/d_{(0\ 0\ n+2)}$ ratio (3.88/3.26 Å) is 1.191, which corresponds to a stage-4 GIC.[50,51] The stage numbers at various potentials are shown in **Table 2**, which indicates that a stage-3 GIC forms at the end of charging (i.e., three free graphene planes between two anion intercalated planes at 2.2 V). Furthermore, the intercalant gallery height (spacing between adjacent graphitic host layers), $d_i$ (Å), can be calculated according to the following equation[10,51]

$$I_c = d_i + 3.35 \times (n-1) = l \times d_{obs} \quad (6)$$

where $I_c$ is the unit cell periodic distance (Å), $l$ is the Miller index of the graphite plane, and $d_{obs}$ is the observed spacing (Å) from the diffractogram. The calculated $d_i$ values are also shown in Table 2. When fully charged, $I_c$ is 16.26 Å and $d_i$ is 9.56 Å. Accordingly, due to the $AlCl_4^-$ intercalation, the graphite interlayer distance expanded by 185%. In the EMICl–$AlCl_3$ IL electrolyte,[10] the graphite electrode showed two dominant peaks at 23.56° and 28.25° after full charge, indicating the formation of a stage-4 GIC. It was also reported that, for the same EMICl–$AlCl_3$ electrolyte, the $d_i$ value was ≈8.95 Å, corresponding to 167% interlayer expansion upon $AlCl_4^-$ intercalation.[52] Only at a low temperature of −10 °C, at which the electrolyte decomposition was postponed and the operation potential could thus be increased to 2.5 V, intercalation of $AlCl_4^-$ up to stage 3 was achievable.[53] A stage-4 GIC was also found for the 1-butyl-3-methylimidazolium–$AlCl_3$ IL electrolyte at room temperature.[54] The comparison results reveal that the

**Table 2.** Stage numbers and gallery height values for graphite cathode acquired using in situ synchrotron XRD at various charge–discharge potentials in IL electrolyte with $AlCl_3$/4-ethylpyridine molar ratio of 1.3.

| Potential [V] | $d_{(0\,0\,n+2)}$ [Å] | $d_{(0\,0\,n+1)}$ [Å] | $d_{(0\,0\,n+1)}/d_{(0\,0\,n+2)}$ | Stage-X | $d_i$ [Å] |
|---|---|---|---|---|---|
| 1.7 | 3.260 | 3.880 | 1.191 | 4 | 9.35 |
| 1.8 | 3.251 | 4.021 | 1.237 | 3 | 9.384 |
| 1.9 | 3.248 | 4.037 | 1.242 | 3 | 9.448 |
| 2.0 | 3.242 | 4.042 | 1.247 | 3 | 9.468 |
| 2.1 | 3.239 | 4.055 | 1.251 | 3 | 9.52 |
| 2.2 | 3.236 | 4.064 | 1.256 | 3 | 9.556 |
| 2.1 | 3.242 | 4.055 | 1.250 | 3 | 9.52 |
| 2.0 | 3.248 | 4.042 | 1.244 | 3 | 9.468 |
| 1.9 | 3.254 | 4.033 | 1.239 | 3 | 9.432 |
| 1.8 | 3.260 | 4.015 | 1.232 | 3 | 9.36 |
| 1.7 | 3.263 | 3.878 | 1.188 | 4 | 9.34 |

proposed 4-ethylpyridine–$AlCl_3$ IL electrolyte is promising for use in RABs to obtain a high degree of anion intercalation in the graphite electrode. As shown in Figure 7, when the cell is discharged back to 0.1 V, the two XRD peaks recombine into one, reflecting the deintercalation of $AlCl_4^-$. However, the peak shape cannot be completely recovered (back to the initial state of pristine graphite). The broad shoulder suggests that there were some trapped intercalants and/or residual strain in the graphite lattices. This observation is analogous to those reported for other Al//graphite cells using different IL electrolytes.[37,54] It is noted that even after fully charging, the (002) graphite diffraction peak still remains. This is probably due to the less electrolyte/electrode ratio that is used for the in situ XRD pouch cell (rather than that of the three-electrode cell used for other electrochemical measurements). Accordingly, the stage-3 intercalation may be underestimated.

Another advantage of the 4-ethylpyridine–$AlCl_3$ IL is at the anode side. Figure S9 of the Supporting Information compares the SEM morphologies of the Al anodes cycled 20 times in conventional EMICl–$AlCl_3$ ($AlCl_3$/EMICl = 1.3 by mole) and 4-ethylpyridine–$AlCl_3$ ($AlCl_3$/4-ethylpyridine = 1.3 by mole) IL electrolytes. A moss-like structure was found for the former electrolyte, whereas a bulky and relatively smooth deposit formed in the latter electrolyte. Moreover, we observed black precipitates at the bottom of the EMICl–$AlCl_3$ cell after cycling. By contrast, no such precipitates appeared in the 4-ethylpyridine–$AlCl_3$ IL electrolyte. The loose Al deposited from the former electrolyte may easily fall off from the electrode, forming dead Al (i.e., loss of electroactive species and thus reduced cell cyclability). Previous work also showed a similar Al morphology after cycling.[15,51] Repeated dissolution/deposition cycles in EMICl–$AlCl_3$ electrolyte easily leads to roughening of the Al electrode. The morphology of the deposited Al layer is related to the coordination chemistry of the electrolyte and the nucleation/growth routes during electrodeposition. The details of the morphological stability require further investigations.

To evaluate the moisture sensitivity of the above two ILs, the electrolytes were taken out of the glove box and their hydrolytic stability was observed. As shown in **Figure 8**a,b, the conventional EMICl–$AlCl_3$ IL reacted violently with moisture and even created smoke, whereas the 4-ethylpyridine–$AlCl_3$ IL was rather stable under an ambient atmosphere. Figure 8c shows the charge–discharge curves of an Al//graphite open cell with the 4-ethylpyridine–$AlCl_3$ IL electrolyte measured under air. The obtained graphite capacities were ≈80 mAh $g^{-1}$ at 50 mA $g^{-1}$ and ≈22 mAh $g^{-1}$ at 300 mA $g^{-1}$. These capacities are only slightly lower than those measured in the $N_2$-filled glove box. Although the discharge voltage is lower than that found inside the glove box, stable charge–discharge properties can be obtained. By contrast, as shown in Figure S10 of the Supporting Information, the EMICl–$AlCl_3$ cell cannot operate under ambient conditions. Figure 8d shows the cycling stability of the 4-ethylpyridine–$AlCl_3$ cell measured under air. After 100 cycles, the capacity retention was ≈75%. The moisture insensitivity of the 4-ethylpridine–$AlCl_3$ IL is associated with the lack of $Al_2Cl_7^-$ and the active $Al^{3+}$ centers being shielded by the 4-ethylpyridine neutral ligands. The low moisture sensitivity of the 4-ethylpyridine–$AlCl_3$ IL can reduce the required environmental control for electrolyte preparation and cell assembly and reduce the safety threat even if the battery packaging is punctured.

It is important to control IL electrolyte corrosion for RABs, for their shelf life. The dissolution of the current collectors, terminals, and containers can degrade battery performance and even lead to unexpected failure and safety problems. In **Figure 9**, the corrosion properties of EMICl–$AlCl_3$ ($AlCl_3$/EMICl = 1.3 by mole) and 4-ethylpyridine–$AlCl_3$ ($AlCl_3$/4-ethylpyridine = 1.3 by mole) ILs toward Al, Cu, Ni, and carbon-fiber paper are compared. The four substances were immersed in the ILs at 60 °C (to accelerate the reaction) for 10 days. For Al, very serious corrosion was found in the former IL. The sample was clearly dissolved and the surface was severely etched (Figure 9a). Similar corrosion phenomena were also reported in the literature.[55,56] By contrast, the Al disk was mostly immune to the 4-ethylpyridine–$AlCl_3$ IL. No significant morphology change was observed after the immersion test. Figure 9b,c indicates that for Cu and Ni, a clearly lower degree of corrosion was found for the 4-ethylpyridine–$AlCl_3$ IL. The anodic polarization data shown in Figure S11 of the Supporting Information also confirm the much lower dissolution rate of Cu and Ni in the 4-ethylpyridine–$AlCl_3$ IL. The carbon-fiber paper is the only material that could withstand the high corrosivity of EMICl–$AlCl_3$ IL, as shown in Figure 9d. The chemical benignity of the 4-ethylpyridine–$AlCl_3$ IL can be attributed to the absence of highly corrosive $Al_2Cl_7^-$.[40–42] The $[AlCl_2(4\text{-ethylpridine})_2]^+$ and $[AlCl_2(4\text{-ethylpyridine})]^+$ cations are less likely to attack metals. Accordingly, the use of this IL electrolyte can not only minimize corrosion damage to battery production facilities but also improve cell reliability and service life.

## 3. Conclusions

A new 4-ethylpyridine–$AlCl_3$ IL electrolyte was proposed for the Al//graphite RAB. An $AlCl_3$ to 4-ethylpyridine molar ratio

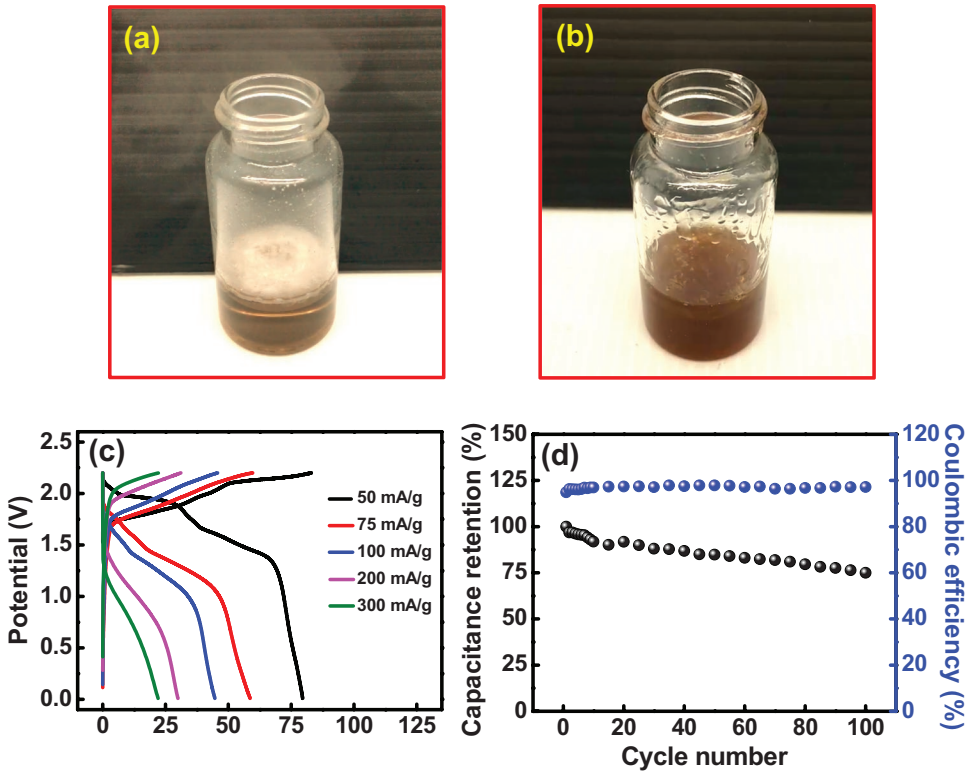


**Figure 8.** Moisture sensitivity of a) EMICl–$AlCl_3$ IL and b) 4-ethylpyridine–$AlCl_3$ IL upon exposure to humid air. c) Galvanostatic charge–discharge curves and d) cycling stability data of Al//graphite cell containing IL electrolyte with $AlCl_3$/4-ethylpyridine molar ratio of 1.3 measured under an ambient atmosphere.

of ≈1.3 was found to be the optimal composition for graphite capacity (≈95 mAh $g^{-1}$ at 25 mA $g^{-1}$) and rate capability. This is the first work to demonstrate an $Al_2Cl_7^-$-free IL electrolyte for RAB applications. In situ synchrotron X-ray diffraction together with XPS and EDS mapping confirmed that a stage-3 GIC forms at the end of charging and that the deintercalation of $AlCl_4^-$ occurs upon discharging. Due to the absence of $Al_2Cl_7^-$ and the use of the neutral 4-ethylpyridine ligand, the 4-ethylpridine–$AlCl_3$ IL showed considerably lower corrosivity toward Al, Cu, and Ni electrodes compared with that of the conventional EMICl–$AlCl_3$ IL. Most importantly, the 4-ethylpyridine–$AlCl_3$ IL is moisture-insensitive and thus allows charge–discharge of the Al//graphite open cell under an ambient atmosphere. This kind of IL electrolyte could lead to RABs that have better reliability, less corrosion damage, and fewer safety problems.

## 4. Experimental Section

*Preparation of Ionic Liquid Electrolytes*: An appropriate amount of $AlCl_3$ (99%, Alfa Aesar) was slowly added into 4-ethylpyridine (98%, TCI) to prepare IL electrolytes with various $AlCl_3$ to 4-ethylpyridine ratios. The mixtures were continuously stirred by magnetic paddles for 24 h to ensure uniformity. A conventional RAB electrolyte that consisted of $AlCl_3$ and EMICl (97 wt%, Acros) with a molar ratio of 1.3:1 was also used for comparison. All the electrolytes were mixed and handled in a $N_2$-filled glove box (Innovative Technology Co. Ltd.), where both the moisture and oxygen levels were maintained at below 0.1 ppm. The ionic conductivity and viscosity of the IL electrolytes were measured using a WTW Cond 3210 conductivity meter and a Rheosense μVISC viscometer, respectively.

*Cell Assembly*: The cathode slurry was fabricated by mixing 90 wt% natural graphite powder (100 mesh; Ted Pella Inc.) and 10 wt% poly(vinylidene fluoride) in *N*-methyl-2-pyrrolidone solution. The slurry was pasted onto carbon-fiber paper and vacuum-dried at 80 °C for 3 h. The graphite mass loading is ≈5 mg $cm^{-2}$. Two Al sheets were used as the anode and reference electrodes, respectively in a three-electrode open cell (≈1 mL in volume), which was assembled and tested in the same glove box used for electrolyte preparation. The use of the three-electrode system is to better control and read the cathode potential, since the reference electrode is not polarized during charging/discharging.

*Material and Electrochemical Characterization*: SEM (FEI Inspect F50) and XRD (Bruker D8) were used to examine the electrode morphology and crystallinity, respectively. The electrolyte coordination status was examined using Raman spectroscopy (UniRAM MicroRaman). XPS (VG Sigma Probe) and EDS (Bruker Quantax) were employed to study the chemical composition of the electrodes. CV was performed with a Biologic VSP-300 potentiostat at a potential sweep rate of 1 mV $s^{-1}$ to characterize the electrochemical properties. The charge–discharge performance (in terms of capacity, rate capability, and cycling stability) of the cells was systematically evaluated. All the measurements were conducted at 25 °C.

For the in situ XRD analysis, a pouch cell was adopted. A thin Al foil (≈30 μm), a natural graphite electrode, and a glass fiber membrane were used as the anode, cathode, and separator, respectively. The windows for X-ray penetration were sealed with Kapton tape. The cell was subjected to synchrotron XRD examination during charging/discharging (at a rate of 10 mA $g^{-1}$), which was performed at Beamlines 01 C and 17 A of the National Synchrotron Radiation Research Center, Taiwan. The 2D diffraction signals were collected using a Mar345 image plate detector and then converted to 1D patterns using the software package Fit2D.

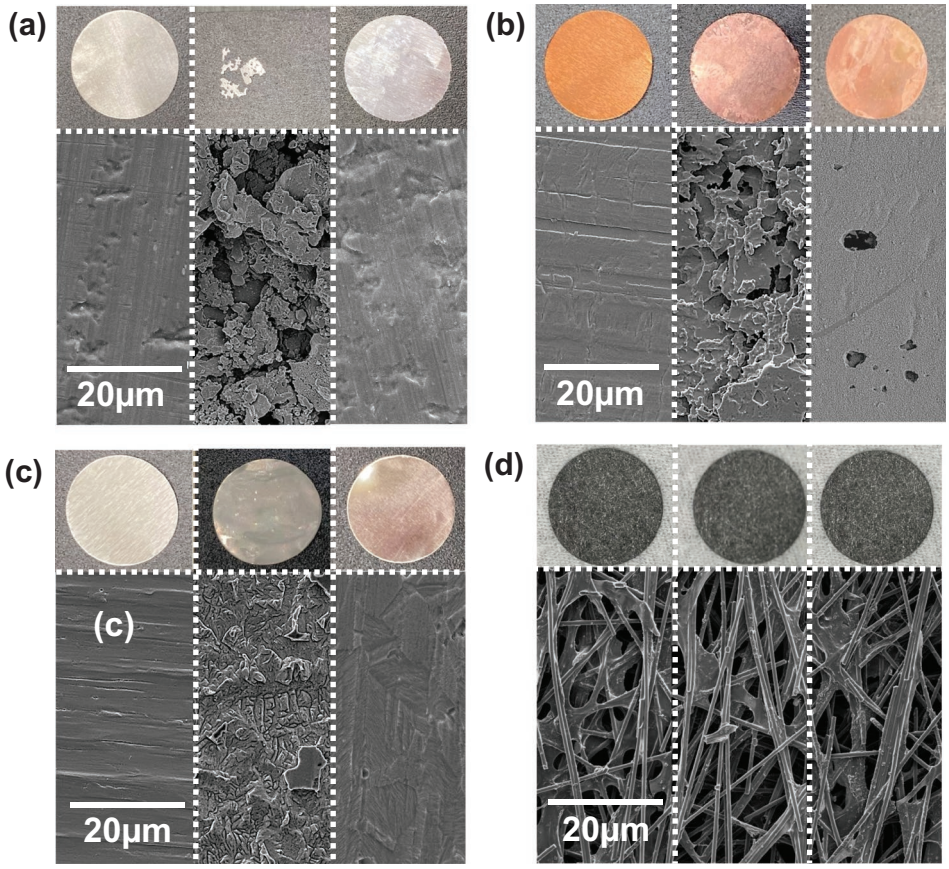


**Figure 9.** a) Al, b) Cu, c) Ni, and d) carbon-fiber paper electrodes before (left side) and after being immersed in EMICl–$AlCl_3$ IL (center) and 4-ethylpyridine–$AlCl_3$ IL (right side) at 60 °C for 10 days. The upper and lower images are taken using digital camera and SEM, respectively.

## Supporting Information

Supporting Information is available from the Wiley Online Library or from the author.

## Acknowledgements

The financial support provided for this work by the Ministry of Science and Technology (MOST) of Taiwan is gratefully appreciated.

## Conflict of Interest

The authors declare no conflict of interest.

## Keywords

air-stable, Al/graphite cells, corrosion, electrolyte design, in situ X-ray diffraction

Received: November 16, 2019
Revised: January 4, 2020
Published online:

[1] B. Dunn, H. Kamath, J. M. Tarascon, *Science* **2011**, *334*, 928.
[2] D. Larcher, J. M. Tarascon, *Nat. Chem.* **2015**, *7*, 19.
[3] N. Yabuuchi, K. Kubota, M. Dahbi, S. Komaba, *Chem. Rev.* **2014**, *114*, 11636.
[4] J. Y. Hwang, S. T Myung, Y. K. Sun, *Chem. Soc. Rev.* **2017**, *46*, 3529.
[5] J. Kalhoff, G. G. Eshetu, D. Bresser, S. Passerini, *ChemSusChem* **2015**, *8*, 2154.
[6] J. B. Goodenough, *Energy Storage Mater.* **2015**, *1*, 158.
[7] P. Huang, P. Ping, K. Li, H. Chen, Q. Wang, J. Wen, J. Sun, *Appl. Energy* **2016**, *183*, 659.
[8] F. Wu, H. Yang, Y. Bai, C. Wu, *Adv. Mater.* **2019**, *31*, 1806510.
[9] G. A. Elia, K. Marquardt, K. Hoeppner, S. Fantini, R. Lin, E. Knipping, W. Peters, J. F. Drillet, S. Passerini, R. Hahn, *Adv. Mater.* **2016**, *28*, 7564.
[10] M. C. Lin, M. Gong, B. Lu, Y. Wu, D. Y. Wang, M. Guan, M. Angell, C. Chen, J. Yang, B. J. Hwang, H. Dai, *Nature* **2015**, *520*, 324.
[11] J. V. Rani, V. Kanakaiah, T. Dadmal, M. S. Rao, S. Bhavanarushi, *J. Electrochem. Soc.* **2013**, *160*, A1781.
[12] C. Zhang, R. He, J. Zhang, Y. Hu, Z. Wang, X. Jin, *ACS Appl. Mater. Interfaces* **2018**, *10*, 26510.
[13] G. Y. Yang, L. Chen, P. Jiang, Z. Y. Guo, W. Wang, Z. P. Liu, *RSC Adv.* **2016**, *6*, 47655.
[14] L. Zhang, L. Chen, H. Luo, X. Zhou, Z. Liu, *Adv. Energy Mater.* **2017**, *7*, 1700034.
[15] X. Huang, Y. Liu, H. Zhang, J. Zhang, O. Noonan, C. Yu, *J. Mater. Chem. A* **2017**, *5*, 19416.
[16] N. P. Stadie, S. Wang, K. V. Kravchyk, M. V. Kovalenko, *ACS Nano* **2017**, *11*, 1911.
[17] Z. Liu, J. Wang, H. Ding, S. Chen, X. Yu, B. Lu, *ACS Nano* **2018**, *12*, 8456.

[18] Z. A. Zafar, S. Imtiaz, R. Li, J. Zhang, R. Razaq, Y. Xin, Q. Li, Z. Zhang, Y. Huang, *Solid State Ionics* **2018**, *320*, 70.
[19] X. Zhang, G. Zhang, S. Wang, S. Li, S. Jiao, *J. Mater. Chem. A* **2018**, *6*, 3084.
[20] S. Choi, H. Go, G. Lee, Y. Tak, *Phys. Chem. Chem. Phys.* **2017**, *19*, 8653.
[21] J. Tu, H. Lei, Z. Yu, S. Jiao, *Chem. Commun.* **2018**, *54*, 1343.
[22] S. Wang, S. Jiao, J. Wang, H. S. Chen, D. Tian, H. Lei, D. N. Fang, *ACS Nano* **2017**, *11*, 469.
[23] T. Mor, Y. Orikasa, K. Nakanishi, K. Chen, M Hattori, T Ohta, Y Uchimoto, *J. Power Sources* **2016**, *313*, 9.
[24] Y. Hu, B. Luo, D. Ye, X. Zhu, M. Lyu, L. Wang, *Adv. Mater.* **2017**, *29*, 1606132.
[25] Z. Li, B. Niu, J. Liu, J. Li, F. Kang, *ACS Appl. Mater. Interfaces* **2018**, *10*, 9451.
[26] J. Wang, Y. Yamada, K. Sodeyama, C. H. Chiang, Y. Tateyama, A. Yamada, *Nat. Commun.* **2016**, *7*, 12032.
[27] E. P. Roth, C. J. Orendorff, *Interface Mag.* **2012**, *21*, 45.
[28] S. Jiao, H. Lei, J. Tu, J. Zhu, J. Wang, X Mao, *Carbon* **2016**, *109*, 276.
[29] S. Wang, K. V. Kravchyk, F. Krumeich, M. V. Kovalenko, *ACS Appl. Mater. Interfaces* **2017**, *9*. 28478.
[30] Z. Li, J. Liu, B. Niu, J. Li, F. Kang, *Small* **2018**, *14*, 1800745.
[31] D. Y. Wang, C. Y. Wei, M. C. Lin, C. J. Pan, H. L. Chou, H. A. Chen, M. Gong, Y. Wu, C. Yuan, M Angell, Y. J. Hsieh, Y. H. Chen, C. Y. Wen, C. W. Chen, B. J. Hwang, C. C. Chen, H. Dai, *Nat. Commun.* **2017**, *8*, 14283.
[32] Y. Wu, M. Gong, M. C. Lin, C. Yuan, M. Angell, L. Huang, D. Y. Wang, X. Zhang, J. Yang, B. J. Hwang, H. Dai, *Adv. Mater.* **2016**, *28*, 9218.
[33] M. Angell, C. J. Pan, Y. Rong, C. Yuan, M. C. Lin, B. J. Hwang, H. Dai, *Proc. Natl. Acad. Sci. USA* **2017**, *114*, 834.
[34] C. Wang, J. Li, H. Jiao, J. Tu, S. Jiao, *RSC Adv.* **2017**, *7*, 32288.
[35] H. Jiao, C. Wang, J. Tu, D. Tian, S. Jiao, *Chem. Commun.* **2017**, *53*, 2331.
[36] J. Li, J. Tu, H. Jiao, C. Wang, S. Jiao, *J. Electrochem. Soc.* **2017**, *164*, A3093.
[37] Y. Song, S. Jiao, J. Tu, J. Wang, Y. Liu, H. Jiao, X. Mao, Z. Guo, D. J. Fray, *J. Mater. Chem. A* **2017**, *5*, 1282.
[38] C. Y. Chen, T. Tsuda, S. Kuwabata, C. L. Hussey, *Chem. Commun.* **2018**, *54*, 4164.
[39] P. Wasserscheid, T. Welton, *Ionic Liquids in Synthesis*, Wiley-VCH Verlag GmbH & Co. KGaA, Germany **2008**.
[40] P. C. Lin, J. K. Chang, J. R. Chen, W. T. Tsai, M. J. Deng, I. W. Sun, *Electrochem. Commun.* **2010**, *12*, 1091.
[41] P. C. Lin, I. W. Sun, J. K. Chang, C. J. Su, J. C. Lin, *Corros. Sci.* **2011**, *53*, 4318.
[42] Y. Zhang, S. Liu, Y. Ji, J. Ma, H. Yu, *Adv. Mater.* **2018**, *30*, 1706310.
[43] H. Xu, T. Bai, H. Chen, F. Guo, J. Xi, T. Huang, S. Cai, X. Chu, J. Ling, W. Gao, Z. Xu, C. Gao, *Energy Storage Mater.* **2019**, *17*, 38.
[44] M. C. Huang, C. H. Yang, C. C. Chiang, S. C. Chiu, Y. F. Chen, C. Y. Lin, L. Y. Wang, Y. L. Li, C. C. Yang, W. S. Chang, *Energies* **2018**, *11*, 2760.
[45] Y. Fang, K. Yoshii, X. Jiang, X. G. Sun, T. Tsuda, N. Mehio, S. Dai, *Electrochim. Acta* **2015**, *160*, 82.
[46] A. S. Childress, P. Parajuli, J. Zhu, R. Podila, A. M. Rao, *Nano Energy* **2017**, *39*, 69.
[47] C. Liu, Z. Liu, Q. Li, H. Niu, C. Wang, Z. Wang, B. Gao, *J. Power Sources* **2019**, *438*, 226950.
[48] H. M. A. Abood, A. P. Abbott, A. D. Ballantynea, K. S. Rydera, *Chem. Commun.* **2011**, *47*, 3523.
[49] Y. Gao, C. Zhu, Z. Chen, G Lu, *J. Phys. Chem. C* **2017**, *121*, 7131.
[50] X. Zhang, N. Sukpirom, M. M. Lerner, *Mater. Res. Bull.* **1999**, *34*, 363.
[51] G. A. Elia, I. Hasa, G. Greco, T. Diemant, K. Marquardt, K. Hoeppner, R. J. Behm, A. Hoell, S. Passerini, R Hahn, *J. Mater. Chem. A* **2017**, *5*, 9682.
[52] G. Greco, D. Tatchev, A. Hoell, M. Krumrey, S. Raoux, R. Hahn, G. A. Elia, *J. Mater. Chem. A* **2018**, *6*, 22673.
[53] C. J. Pan, C. Yuan, G. Zhu, Q. Zhang, C. J. , Huang, M. C. Lin, M. Angell, B. J. Hwang, P. Kaghazchi, H. Dai, *Proc. Natl. Acad. Sci. USA* **2018**, *115*, 5670.
[54] Z. Yu, J. Tu, C. Wang, S. Jiao, *ChemistrySelect* **2019**, *4*, 3018.
[55] H. Sun, W. Wang, Z. Yu, Y. Yuan, S. Wang, S. Jiao, *Chem. Commun.* **2015**, *51*, 11892.
[56] F. Wu, N. Zhu, Y. Bai, Y. Gao, C. Wu, *Green Energy Environ.* **2018**, *3*, 71.